Millimeter-wave Generation Based on Four Phase-shifted Sampled Moiré Grating Dual-wavelength DFB Laser

Yizhe Fan, Bocheng Yuan, Mohanad Al-Rubaiee, Yiming Sun, Simeng Zhu, Jehan Akbar, John Marsh, *Life Fellow, IEEE*, and Lianping Hou, *Senior Member, IEEE*

***Abstract*—We propose and demonstrate experimentally a dual-wavelength DFB laser based on a four phase-shifted sampled Moiré grating (4PS-SMG). By designing 4PS gratings with different sampling periods on each side of the ridge waveguide, an equivalent introduction of two π phase shifts within the cavity is achieved, enabling the device to exhibit dual-wavelength lasing. The sampling periods of the 4PS-SMG on each side of the ridge waveguide are 4668 nm and 4609 nm, respectively. The 59 nm difference in sampling periods can be realized with high quality through electron beam lithography (EBL). Additionally, the sidewall grating structure requires only one exposure to define both the ridge waveguide and the grating, avoiding issues related to misalignment between the grating and the ridge waveguide. When injecting current into the DFB laser within the 130 mA to 210 mA range, the device delivers exceptional dual-wavelength performance, featuring a power difference of less than 2 dB between the two primary modes. The device provides a high-quality radio frequency (RF) signal at 39.4 GHz, with a narrow linewidth of around 5.0 MHz.**

***Index Terms*—Millimeter-wave, dual-wavelength DFB laser, DFB semiconductor laser, sampled Moiré grating.**

I. INTRODUCTION

Innovative approaches for millimeter-wave (MMW) signal generation have gained significant attention, particularly in the context of 5G communications, radio systems, and vehicular networks [1, 2]. Researchers have explored both electronic and photonic methods for MMW signal generation. Photonic methods have distinct advantages, offering a more compact system design and better noise characteristics compared to their electronic counterparts [3-6]. Among the photonic solutions, the utilization of monolithic dual-mode laser sources has emerged as a promising avenue due to their compact form factor and cost-effective fabrication.

For DFB lasers, the grating is a key function determining the optical output signal. Dual-wavelength lasers (DWLs) have been reported using different grating modulation schemes such as chirp and apodization [7, 8]. In addition, Sampled Bragg grating based on reconstructed equivalent chirp (REC) technology has also been proposed and utilized in DWLs [9]. These methods require two actual and tangible π phase shifts to enable dual-mode lasing. However, Moiré gratings (MGs), formed by superimposing two Bragg gratings with slight period differences, exhibit perfect apodization with a cosine profile, resulting in a corresponding π phase shift in the cavity [10]. To generate MMW signals with conventional MGs, a very slight difference in grating periods (~0.1 nm) is needed, which can be challenging to achieve in practice. Recent literature reports that sampled Moiré gratings (SMG) are an effective approach for addressing the challenge of fabricating gratings with extremely small period differences. Using SMGs, the wavelength control precision required for a conventional MG is relaxed from the nanometer scale to the micrometer scale, substantially mitigating the influence of manufacturing inaccuracies. The achievement of single wavelength lasing in such a device was realized with a 20 nm difference between the two sampling periods [11, 12]. In reference [13], the potential for dual-wavelength lasing using conventional Sampled Moiré Gratings (C-SMG) is discussed, although it remains in the simulation phase. However, the grating coupling coefficient κ of a conventional sampled Moiré grating (C-SMG) in the $\pm1^{st}$ channel is only $1/\pi$ of that of a uniform Bragg grating (UBG). In addition, the presence of the 0^{th} channel in a C-SMG can also impact the performance of the device.

In this paper, we first introduce a four-phase-shifted sampled Moiré grating (4PS-SMG) design for dual-wavelength lasing. Utilizing the 4PS-SMG, we require a sampling period difference of 59 nm between the two superimposed 4PS gratings, which can readily be defined using Electron Beam Lithography (EBL). Meanwhile, in contrast with a C-SMG, the κ of the $+1^{st}$ channel in the 4PS structure can be as high as 0.9 times that of the UBG, and the 0^{th} channel is effectively suppressed [14]. Moreover, the DFB laser relies on a sidewall grating structure, enabling simultaneous fabrication of the ridge waveguide and gratings. In contrast to the traditional buried grating DWL approach, our method requires only a single step of Metal Organic Chemical Vapor Deposition (MOCVD) and one step of III-V

This work was supported by the U.K. Engineering and Physical Sciences Research Council (EP/R042578/1).

Yizhe Fan, Bocheng Yuan, Mohanad Al-Rubaiee, Yiming Sun, Simeng Zhu, Jehan Akbar, John H. Marsh, and Lianping Hou are with the James Watt School of Engineering, University of Glasgow, Glasgow G12 8QQ, U.K. (e-mail: 2636405F@student.gla.ac.uk; 2644187y@student.gla.ac.uk; m.al-rubaiee.1@research.gla.ac.uk; 2465522s@student.gla.ac.uk; 2635935z@student.gla.ac.uk; Jehan.Akbar@glasgow.ac.uk; John.Marsh@glasgow.ac.uk; Lianping.Hou@glasgow.ac.uk).

material etching, streamlining the entire device fabrication process. Simultaneously, our approach mitigates the problem of misalignment between the ridge waveguide and the grating, an issue that can arise with multiple exposures [15].

II. Design and Analysis

The schematic of C-SMG and 4PS-SMG is illustrated in Fig. 1(a). The C-SMG structure comprises both grating and non-grating sections, with each section being half of the sampling period in length, resulting in a coupling efficiency for the +1 order sub-grating channel approximately 1/π times that of a uniform grating. In contrast, the 4PS-SMG structure divides sampling period into four equal sections, with each adjacent section featuring a π/2-phase shift. This yields a coupling efficiency for the +1 order sub-grating channel approximately 0.9 times that of a UBG. The transfer Matrix Method (TMM) was used to calculate the reflection spectrum of the UBG, conventional sampled and 4PS sampled gratings in Fig. 1(b). Notably, the 4PS sampled structure not only eliminates the 0th order channel but also enhances the +1 order sub-grating channel by approximately three times compared to the conventional sampled structure. In both SMG types, different sampling periods, i.e., P_1 and P_2, are employed on each side of the ridge waveguide to create an equivalent index modulation along the DFB laser cavity.

For mathematical analysis, a seed grating with a period of Λ_0 and a duty cycle of 50% is assumed. The sampling periods on each side of the grating are denoted as P_1 and P_2. The initial phase of the seed grating is denoted as φ_0, while the phases of the two 4PS-SBGs are represented by φ_{s1} and φ_{s2}. The grating recess is d and the ridge width is W as shown in the bottom of Fig. 1(a). Utilizing Fourier analysis, we can extract the +1st order sub-grating period as [13]:

$$\Lambda_{+1}(x) = \begin{cases} \Lambda_1 = P_1\Lambda_0/(P_1+\Lambda_0) & \left(-\frac{W+d}{2} < x < 0\right) \\ \Lambda_2 = P_2\Lambda_0/(P_2+\Lambda_0) & \left(0 < x < \frac{W+d}{2}\right) \end{cases} \quad (1)$$

Using the period of the +1st order sub-grating, we can formulate the relative permittivity perturbation. Following the principles of coupled mode theory [16], we isolate the phase-matching component of the perturbation for each sampling structure, allowing us to derive the coupling coefficient of the +1st order sub-grating within the SMG. The variation in the coupling coefficient exhibits a cosine function with a periodicity of Λ_c and an initial phase offset of $(\varphi_2 - \varphi_1)$ along the waveguide direction. A comprehensive analysis and in-depth discussion on this topic can be found in [15]. As a result, we can find the equivalent index modulation Δn_e for the +1st order sub-grating channel in the SMG as follows:

$$\Delta n_e(z) = \Delta n F_{+1} cos\left(\frac{2\pi z}{\Lambda_s} + \frac{\varphi_1+\varphi_2}{2}\right) cos\left(\frac{2\pi z}{\Lambda_c} - \frac{\varphi_2-\varphi_1}{2}\right) \quad (2)$$

where $\Lambda_c = 2\Lambda_1\Lambda_2/(\Lambda_2-\Lambda_1)$, and $\Lambda_s = 2\Lambda_1\Lambda_2/(\Lambda_1+\Lambda_2)$, $\varphi_1 = \varphi_0 + \varphi_{s1}$, and $\varphi_2 = \varphi_0 + \varphi_{s2}$. F_{+1} is the +1st order Fourier coefficient of the sampling structure. Because the two sampling periods are close in value, there is a significant disparity between the values of Λ_s and Λ_c ($\Lambda_c \gg \Lambda_s$).

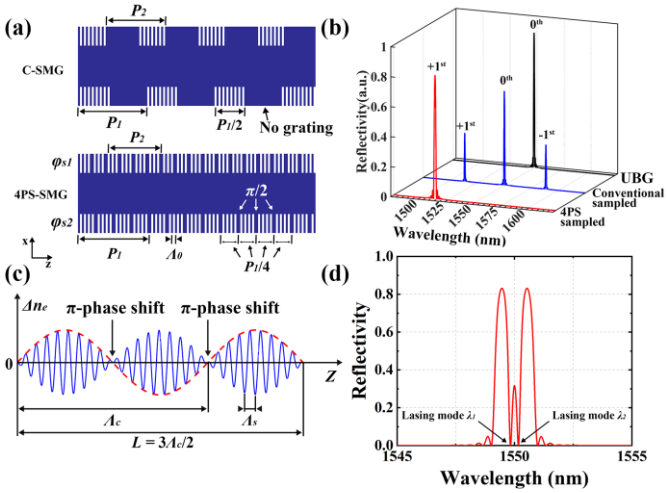

Fig. 1. (a) Top view of the C-SMG and 4PS-SMG. **(b)** Calculated reflectivity of UBG, conventional, and 4PS sampled gratings. **(c)** Equivalent refractive index modulation of the +1 order sub-grating inside the grating cavity based on a SMG. **(d)** Calculated reflection spectrum of 4PS-SMG.

Therefore, the mathematical form of the refractive index modulation of the +1st order sub-grating in SMG becomes an envelope function with the rapid changing component having a period of Λ_s and the slowly changing envelope a period of Λ_c. In addition, the equivalent refractive index creates a π-phase shift where the cosine variation of the envelope meets a crossover [9].

Fig. 1(c) shows the equivalent index modulation within the cavity. The cavity length is set to be $L = 1.5 \times \Lambda c$. The rapidly oscillating component (with the period Λ_s) defines the position of the center of the Bragg reflection band as $\lambda = 2n_{eff}\Lambda_s$, where n_{eff} is the effective index and λ is the center Bragg wavelength. The initial phase of the envelope indicates a phase difference of π between two sampling structures (φ_{s1} and φ_{s2}). Consequently, this design creates two π-phase shift points within the cavity, resulting in dual longitudinal mode lasing.

To validate these observations, simulations were carried out using TMM, as depicted in Fig. 1(d). The coupling coefficient varies along the cavity with a period Λ_c, while the initial phase difference between the two sampling structures is π. The desired lasing modes both fall within the central stop band, as shown in Fig. 1(d).

III. Fabrication and Experimental Results

The proposed DFB laser is fabricated in the AlGaInAs/InP-based material system. The multiple quantum well (MQW) structure consists of 5 quantum wells (QW) and 6 quantum barriers (QB). Each QW has a thickness of 6 nm with a compressive strain of 1.2%, while the QB has a thickness of 10 nm with a tensile strain of -0.3% [17].

A schematic of the whole device is shown in Fig. 2(a). The SMG-based DFB section is 1100 μm long ($L = 1.5 \times \Lambda c$). The device also contains two 400-μm-long semiconductor optical amplifiers (SOAs) on either side of the DFB section

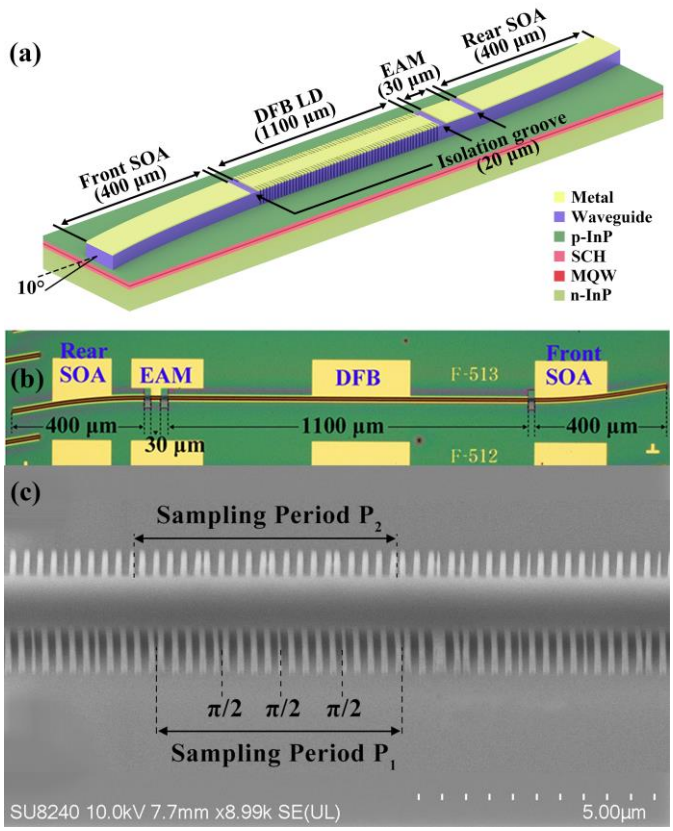

Fig. 2. (a) Schematic of the dual-wavelength DFB laser based on SMG structures. **(b)** Optical microscope picture of the device. **(c)** SEM image of the ridge waveguide and sidewall grating defined by HSQ.

for gain equalization, because adjustment of the SOA currents can slightly alter the photon distribution inside the cavity. The curved waveguides are designed with tilt angles of 10° (radius equals 1730 μm), which also eliminate the FP modes caused by the facet reflection. The 30-μm-long electro-absorption modulator (EAM) is included to adjust the output power and the phase of the two lasing modes when applying a suitable reverse voltage, ensuring the two longitudinal modes have relatively equal intensities. Between each component, there is a 20 μm wide electrical isolation grove created by etching the heavily doped 200 nm thick InGaAs contact layer and 50 nm 1.3Q layer. The isolation resistance is around 10 kΩ. A micrograph of the whole fabricated device is shown in Fig. 2(b).

Fig. 2(c) displays the hydrogen silsesquioxane (HSQ) grating mask prior to the dry etching process. The ridge waveguide has a width of 2.5 μm, while the grating recesses are 0.6 μm on both sides of the ridge. The seed grating has a period of 257 nm. The sampling periods, P_1 and P_2, are 4.609 μm and 4.668 μm respectively on either side of the ridge waveguide. The SMG structure is realized based on 4PS sampled gratings. In each sampling period, it is divided into 4 parts with π/2-phase shift to the adjacent section. The initial phase of the sampled grating at each side has a difference of π according to the previous analysis.

The detailed fabrication process can be found in [9]. The completed chip was cleaved into bars, soldered to a copper sub-mount using indium, and characterized under continuous wave (CW) conditions at 20 °C. The cooling system employed a thermoelectric cooler (TEC) in conjunction with a copper heat sink that integrates water cooling. It is important to note that all the measured results are obtained from the front side of the SOA.

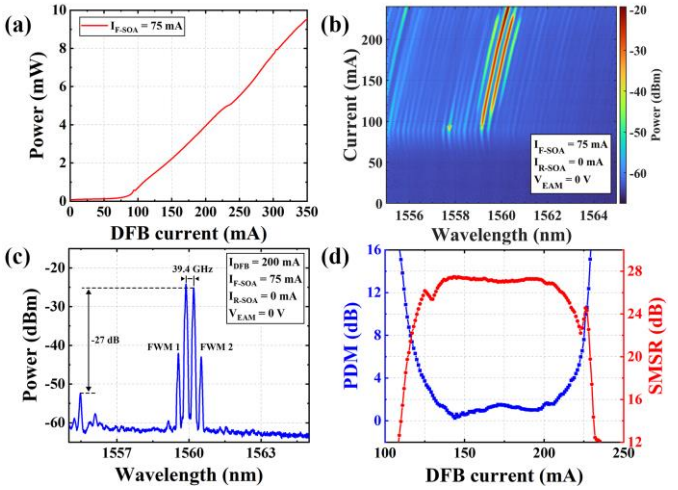

Fig. 3. (a) *P-I* curve when $I_{F\text{-}SOA}$ =75 mA, $I_{R\text{-}SOA}$= 0 mA, and V_{EAM} =0 V. **(b)** 2D optical spectrum vs I_{DFB} when $I_{F\text{-}SOA}$ = 75 mA, $I_{R\text{-}SOA}$ = 0 mA, and V_{EAM} = 0 V. **(c)** Dual-mode operation spectrum when I_{DFB} =200 mA. **(d)** PDM and SMSR vs I_{DFB}.

The power-current (*P-I*) curves were measured with the front SOA current ($I_{F\text{-}SOA}$) at 75 mA, the rear SOA current ($I_{R\text{-}SOA}$) at 0 mA and the voltage of EAM (V_{EAM}) at 0 V. As shown in Fig. 3(a), the threshold current is 80 mA. The output power can reach 9.6 mW at a DFB current (I_{DFB}) of 350 mA. The comparatively lower output power may result from the misalignment between the peak gain of the front SOA (1523 nm) at 75 mA and the center wavelength of the dual-wavelength DFB laser, which is approximately 1560 nm (refer to Fig. 3(c)). Addressing this issue can be achieved by optimizing the length of the SOA.

In Fig. 3(b), the 2D optical spectrum is displayed as a function of I_{DFB}. The device exhibited very stable dual-mode lasing behavior within the I_{DFB} range of 130 mA to 210 mA, with $I_{F\text{-}SOA}$ =75 mA, $I_{R\text{-}SOA}$=0 mA, and V_{EAM} =0 V. The spectra reveal the presence of a four-wave mixing (FWM) signal, indicating a good phase relationship between the two main lasing modes. The TE_{01} leaky mode, which is manifest around 1555 nm, can be attributed to the asymmetry of the dual-sided grating within the SMG cavity. This asymmetry leads to mode conversion between the forward TE_{00} mode and the backward TE_{01} mode [15]. Fortunately, this leakage mode does not affect the performance of the DWL devices. A detailed optical spectrum at I_{DFB} = 200 mA is depicted in Fig. 3(c). The corresponding optical frequency difference between the two lasing modes is 39.4 GHz. The side mode suppression ratio (SMSR) is measured as 27 dB. The power difference between the two modes (PDM) and the SMSR are shown in Fig. 3(d). The device shows very stable dual-mode lasing over a range of 80 mA (130 mA-210 mA), where the PDM is less than 2 dB and the SMSR exceeds 25 dB.

Fig. 4(a) shows the RF signal with I_{DFB} set to 200 mA, $I_{F\text{-}SOA}$ to 75 mA, $I_{R\text{-}SOA}$ at 0 mA, and V_{EAM} at 0 V. The RF signal has a 30 dB peak over the noise floor, with a resolution bandwidth (RBW) value set at 1 MHz. The center frequency is 39.4 GHz which corresponds to the wavelength spacing of dual-mode lasing as shown in Fig. 3(c). As demonstrated in the inset of Fig. 4(a), the beat note of the RF signal (black dots) was fitted using a Lorentz profile (red line), where the RBW of the electrical spectrum analyzer (ESA) was set to 10 kHz and the span was 400 MHz. The –3 dB bandwidth is 4.7 MHz according to the fitted profile when I_{DFB} is 200 mA. The –3 dB linewidth as a function of I_{DFB} is shown in Fig. 4(b). The device shows a stable linewidth around 5 MHz when I_{DFB} is within the range of 120-220 mA. The device shows a typical trend of the linewidth reducing as I_{DFB} is increased. When I_{DFB} falls outside the dual-mode operation range, the PDM experiences a significant increase, resulting in a corresponding broadening of the linewidth. The narrowest linewidth is 4.07 MHz when I_{DFB} is 205 mA.

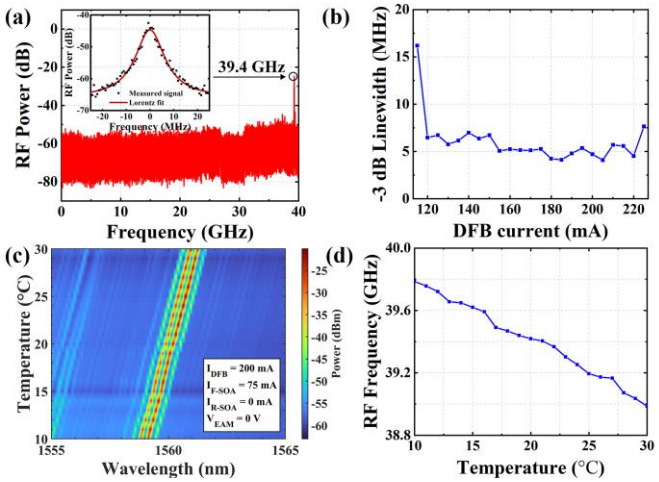

Fig. 4. (a) Measured full span RF signal and zoomed-in RF peak with Lorentz fit (inset). **(b)** Measured –3 dB linewidth vs I_{DFB}. **(c)** 2D optical spectrum vs temperature when I_{DFB}= 200 mA. **(d)** RF frequency vs temperature when I_{DFB}= 200 mA.

Fig. 4(c) illustrates the wavelength shift over a working temperature range from 10 °C to 30 °C. The temperature tuning coefficient of the wavelength is 0.105 nm/°C. The corresponding RF frequency is also measured, as shown in Fig. 4(d). The wavelength separation between the two primary modes remains constant, whereas the center wavelength experiences a redshift with increasing temperature. The RF frequency, as a result, changes from 39.8 GHz to 39.0 GHz. The minor deviations observed in the RF frequency, as compared to a straight line, can be attributed to factors such as the noise generated by the DC source and external environmental variables, including temperature fluctuations within the device and mechanical vibrations. Implementing a battery-powered DC source, enhancing temperature control, and ensuring a more stable measurement platform with reduced vibration, along with packaging the device, would likely mitigate this phenomenon.

IV. Conclusion

This is the first proposal of a DWL utilizing a sidewall 4PS-SMG. The approach requires only a single step of MOCVD and a solitary step of III-V dry etching, resulting in a substantial simplification of the fabrication processes. The lasers displayed stable dual-mode operation over a current range of 80 mA. The generated RF frequency was measured to be around 39.4 GHz, with a linewidth of approximately 5.0 MHz. These experimental findings underline the potential of the device as a highly integrated, user-friendly source of MMW.

References

[1] T. S. Rappaport, et al., "Overview of millimeter wave communications for fifth-generation (5G) wireless networks-with a focus on propagation models", *IEEE Trans. Antennas Propag.*, vol. 65, pp. 6213-6230, Dec. 2017

[2] J. Wang, et al, "Networking and Communications in Autonomous Driving: A Survey," *IEEE Communications Surveys & Tutorials*, vol. 21, no. 2, pp. 1243-1274, 2019.

[3] M. J. Fice, et al., "146-GHz millimeter wave radio-over-fiber photonic wireless transmission system", *Opt. Exp.*, vol. 20, no. 2, pp. 1769-1774, Jan. 2012.

[4] F. van Dijk, et al., "Quantum dash mode-locked lasers for millimeter wave signal generation and transmission", Proc. 23rd Annu. Meeting IEEE Photon. Soc., 2010, pp. 187-188.

[5] T. P. McKenna, et al., "Photonic Millimeter-Wave System for High-Capacity Wireless Communications", *Johns Hopkins APL Technical Digest*, vol. 33, pp. 57-67, 2015.

[6] B. Razavi, "Design of Millimeter-Wave CMOS Radios: A Tutorial", *IEEE. Transactions on Circuits and Systems I: Regular Papers*, vol. 56, pp. 4-16, Jan. 2009.

[7] B. Lin, et al., "Inverse-Gaussian apodized fiber Bragg grating for microwave generation," 2010 Photonics Global Conference, Singapore, 2010, pp. 1-3.

[8] B. Yuan, et al., "A Dual-Wavelength DFB Laser Based on Reconstruction-Equivalent-Chirp Technology for Millimeter-Wave Generation," 2020 International Conference on UK-China Emerging Technologies (UCET), Glasgow, UK, 2020, pp. 1-3.

[9] B. Yuan, et al, "Millimeter wave generation based on monolithic dual-wavelength DFB laser with four phase-shifted sampled grating and equivalent chirp technology," Optics Letters, vol.48, no.19, pp.5093-5096, 2023.

[10] D. C. J. Reid, et al., "Phase-shifted moire grating fibre resonators," *Electron. Lett.*, vol.26, pp. 10-12, Jan. 1990.

[11] M. Chen, et al., "Study on DFB semiconductor laser based on sampled moiré grating integrated with grating reflector," 18th International Conference on Optical Communications and Networks (ICOCN), Huangshan, China, 2019, pp. 1-3.

[12] S. Liu, et al., "Study on the high-power DFB semiconductor laser based on sampled moiré grating," 2020 International Conference on UK-China Emerging Technologies (UCET), Glasgow, UK, 2020, pp. 1-4.

[13] W. Qi, et al., "Dual Wavelength Laser Designed for Locking to Cs-133 Atomic Transitions," 2021 Conference on Lasers and Electro-Optics Europe & European Quantum Electronics Conference (CLEO/Europe-EQEC), Munich, Germany, 2021, pp. 1-1.

[14] J. Li et al., "A Multiexposure Technology for Sampled Bragg Gratings and its Applications in Dual-Wavelength Lasing Generation and OCDMA En/Decoding," *IEEE Photonics Technology Letters*, vol. 21, no. 21, pp. 1639-1641, Nov.1, 2009.

[15] S. Liu, et al., "Planar waveguide moiré grating," *Opt. Express*, vol. 25, no. 21, pp. 24960-24973, 2017.

[16] L. A. Coldren, S. W. Corzine, and M. L. Mashanovitch, "Diode lasers and photonic integrated circuits", John Wiley & Sons, 2012, pp. 353-356.

[17] L. Hou et al., "Subpicosecond Pulse Generation at Quasi-40-GHz Using a Passively Mode-Locked AlGaInAs–InP 1.55-μm Strained Quantum-Well Laser," *IEEE Photonics Technology Letters*, vol. 21, no. 23, pp. 1731-1733, Dec.1, 2009.